Contents

Chapter 1

The Higgs Bosons and the MSSM

This chapter is devoted to introduce the theoretical background to the experimental search presented in this thesis. A brief overview of the Standard Model of particle physics is given in Section 1.1 based on Reference [1]. Among all the extension of the Standard Model, the Minimal Supersymmetric extension of the Standard Model (MSSM) is a theoretically favoured scenario as one of the most predictive framework beyond the Standard Model. The MSSM is introduced in Section 1.2 with focus on its Higgs sector, based on References [2, 3]. Finally, a review of the MSSM Higgs bosons phenomenological aspects which are relevant to the presented search is given in Section 1.3, based on Reference [4].

1.1 The Standard Model of Particle Physics

1.1.1 Introduction

A detailed description of the Standard Model of particle physics may be found in Reference [6], only a brief overview is given in what follows.

The Standard Model (SM) of particle physics is a theory aimed to describe and quantitatively predict the phenomenology of fundamental interactions. At "microscopic" level the spectrum of all interactions between matter and radiation can be understood in terms of three classes of fundamental forces: the strong, the electromagnetic and the weak forces. These interactions are described by a local relativistic quantum field theory, where to each particle is associated a field with suitable transformation properties under the Lorentz group. The theory is based on the principle of gauge invariance, which means invariance under a symmetry transformations that operates on basic internal degrees of freedom and depends on the space-time coordinate. The gravitational force is negligible in atomic and nuclear physics, in fact, quantum effects of gravity are expected at energies corresponding to the Planck mass $E \sim M_{planck}c^2 \sim 10^{19}$ GeV.

The SM is a gauge field theory based on the symmetry group $SU(3)_c \otimes SU(2)_L \otimes U(1)_Y$. The group has $8 + 3 + 1 = 12$ generators with a non trivial commutator algebra. The electromagnetic and weak interactions [7–9] are described by the $SU(2)_L \otimes U(1)_Y$ symmetry group, while the $SU(3)_c$ is the colour group of the theory of strong interactions (QCD) [10]. To each generator of the symmetry group is associated a vector boson which act as mediator of the corresponding interactions. Eight gluons are associated to the $SU(3)_c$ colour generators, while four gauge bosons $W^{\pm}$, Z^0 and γ are associated to the generators of $SU(2)_L \otimes U(1)_Y$. Only the gluons and the photon are massless since the symmetry induced by the other three generators is spontaneously broken. In the SM the spontaneous symmetry breaking is realised by the Higgs mechanism [11–15]. The Higgs boson acts as mediator of a new class of interactions that, at tree level, are coupled in proportion to the particle masses. An Higgs boson with properties that resemble the one of the SM has recently been discovered at the LHC with $m_H \sim 126$ GeV [16, 17].

The fermionic matter fields of the SM are quarks and leptons. Quarks are subject to all SM interactions, each type of quark is a colour triplet and carries electroweak charges, in particular electric charges $+2/3$ for up-type quarks and $-1/3$ for down-type quarks. Leptons are colourless but have electroweak charges, in particular electric charge -1 for charged leptons e, μ and τ (opposite sign charge is intended for respective anti-particle) and charge 0 for neutrinos ν_e, ν_μ and ν_τ. Qarks and leptons are grouped in three "generations" with equal quantum numbers but different masses.

1.1.2 Precision Test and Limitation of the SM

The Standard Model has been successfully tested in a vast number of experiments over a wide range of energies during the last few decades. Precision tests of the electroweak theory performed at LEP, SLC and the Tevatron [20], has confirmed that the couplings of quark and leptons to the weak gauge bosons $W^{\pm}$ and Z are

indeed precisely those prescribed by the gauge symmetry. The accuracy of a few per-mille for these tests implies that, not only the tree level, but also the structure of quantum corrections has been verified. Several other experimental results [19] including rare decays of hadrons provides low-energies test of the Standard Model. The recent discovery of a Higgs boson is also another success of the SM, its mass, spin and couplings are in agreement with expected values from a global fit of electroweak constraints [21].

Among all the parameters of the Standard Model only few of them presents tension with experimental data, the most significant discrepancies are slightly above three standard deviations and are given by: the anomalous magnetic moment of the muon [22], a_μ and the forward-backward asymmetry of top quarks [23], $A_{FB}^{t\bar{t}}$.

In spite of this success, the Standard Model is conceptually unsatisfactory for quite few deficiencies and is widely believed to be an effective theory valid only at the present accessible energies. Beside the fact that it does not include gravitational force, it does not explain the pattern of fermion masses and in its simplest version does not include neutrino masses, it has at least other three conceptual problems which indicates the need for physics Beyond the Standard Model (BSM):

Hierarchy Problem Calculating the radiative correction to the Higgs boson mass, quadratic divergences occur of the order of the cut-off scale Λ, where Λ defines the energy beyond which the theory ceases to be valid and new physics should appear [24]. If the cut-off is chosen to be $\sim M_{Planck}$, then a fine tuning with an unnaturally high precision , $\mathcal{O}(10^{-30})$, should occur to cancel these divergences leaving the Higgs boson with a mass of the order of the electroweak breaking scale, M_{EW}. A question that has no satisfactory answer in the SM is how these cancellations can occur and why $\Lambda >> M_{EW}$, these problems are called the fine-tuning and hierarchy problem [25–27].

Dark Matter The SM does not have a candidate which can explain the large contribution of non-barionic, non-luminous matter to the density of the Universe [28–30]. To be a Dark Matter candidate a particle should be stable, massive and should interact only via very weak interactions.

Unification Problem Another unsatisfactory aspect of the SM is that does not provide the unification of the electroweak and strong interactions, their couplings do not meet at high energies. Considering the successful unification of electromagnetic and weak interaction, the existence of Grand Unified Theory (GUT) has been suggested [31, 32], which predicts the unification of all the three gauge coupling strength at the GUT energy scale, $\Lambda_{GUT} \simeq 10^{16}$ GeV and describes the three forces within a single gauge group with just one coupling constant.

Among all the extension of the SM, Supersymmetry is a theoretically favoured scenario as the most predictive framework beyond the Standard Model. As discussed in Section 1.2, it gives a natural answer to the hierarchy problem, provides a suitable candidate for Dark Matter and predicts unification of the three gauge couplings at GUT energy scale.

1.2 The Minimal Supersymmetric Standard Model

1.2.1 Introduction to the MSSM

Supersymmetry (SUSY) [33–35] was first introduced as a natural way to solve the hierarchy problem. In Supersymmetry a new symmetry that relates bosons to fermions is introduced. The SUSY generators $\mathcal{Q}$ transforms fermion into bosons and vice versa:

$$\mathcal{Q}|\text{Fermion}\rangle = |\text{Boson}\rangle, \quad \mathcal{Q}|\text{Boson}\rangle = |\text{Fermion}\rangle \tag{1.1}$$

In a supersymmetric extension of the SM each of the known fundamental particles is in either a chiral or gauge *supermultiplet* and must have a superpartner with spin differing by 1/2 unit. SUSY naturally solve the hierarchy problem since the quadratic divergent loop contribution to the Higgs mass of the SM particles are cancelled by the loop contribution of the corresponding superpartners. The name of the superpartner of the quarks and leptons are made by adding an "s" to the SM name, standing for scalar. Accordingly, the gauge bosons related to the generator of the group $SU(3)_c \otimes SU(2)_L \otimes U(1)_Y$ should also have a spin 1/2 partner, whose name will be made by adding a "ino" at the end of the SM name. The symbol of superpartners is defined by adding a ($\tilde{}$) to the SM symbol. The SUSY particles share the same couplings with their SM partner, since the left-handed and right-handed components of fermions transform differently under gauge transformations also their superpartner present this feature.

The Minimal Supersymmetric extension of the Standard Model (MSSM) [36–41], is defined by requiring the minimal gauge group (i.e., the SM one) and the minimal particle content: three generation of fermions (without right-handed neutrinos), gauge bosons and two Higgs doublet, each with its own superpartner. Tables 1.1 and 1.2 summarise chiral and gauge supermultiplets in the MSSM. Among the gauge eigenstates summarised in these tables, the superpartner of the Higgs bosons, the *higgsinos* mix with the *wino* and *bino* to give the "ino" mass eigenstates: two charginos $\chi^{\pm}_{1,2}$ and four neutralinos $\chi^{0}_{1,2,3,4}$.

R-parity conservation

The MSSM requires a discrete and multiplicative symmetry called R-parity [35], this symmetry assures barion and lepton number conservation and it is defined as follows:

$$R_p = (-1)^{2s+3B=L} \tag{1.2}$$

where L and B are lepton and barion numbers and s stands for the spin quantum number. The R-parity quantum number has value $+1$ for ordinary SM particles and -1 for their superpartners. This symmetry was first introduced as a simple way to overcome the problem of instability of the proton. Lepton and barion number violation leads, in many cases, to unstable proton with life-time shorter than the experimental lower limit. The conservation of R-parity has also other important phenomenological consequences: SUSY particles are always produced in pairs and decays always in an odd number of SUSY particles. Furthermore, the lightest SUSY

Names	Supermultiplets	Spin 1/2	Spin 0
quark, squarks	Q	$(u_L\ d_L)$	$(\tilde{u}_L\ \tilde{d}_L)$
($\times$ 3 families)	$\bar{u}$	$u_R^\dagger$	$\tilde{u}_R^*$
	$\bar{d}$	$d_R^\dagger$	$\tilde{d}_R^*$
leptons, sleptons	L	$(\nu\ e_L)$	$(\tilde{\nu}\ \tilde{e}_L)$
($\times$ 3 families)	$\bar{e}$	$e_R^\dagger$	$\tilde{e}_R^*$
higgsinos, Higgs	H_1	$(\tilde{H}_1^0\ \tilde{H}_1^-)$	$(H_1^0\ H_1^-)$
	H_1	$(\tilde{H}_2^+\ \tilde{H}_2^0)$	$(H_2^+\ H_2^0)$

Table 1.1: This table is based on Reference [2] and summarise the chiral supermultiplets in the Minimal Supersymmetric Standard Model. The spin-0 fields are complex scalars and the spin-1/2 are left-handed two-component Weyl fermions.

Names	Supermultiplets	Spin 1	Spin 1/2
gluons, gluinos	G_a (a =1,...,8)	g	$\tilde{g}$
W bosons, winos	W_a (a=1,...,3)	$W^\pm\ W^0$	$\tilde{W}^\pm\ \tilde{W}^0$
B boson, bino	B	B^0	$\tilde{B}^0$

Table 1.2: This table is based on Reference [2] and summarise the gauge supermultiplets in the Minimal Supersymmetric Standard Model.

particle, often chosen as one of the neutralinos, is stable and provides a suitable candidate for dark matter.

The Soft SUSY Breaking

In case Supersymmetry is an exact symmetry of nature, the SM particles and their relative superpartners should have the same mass and quantum numbers except for the spin. However, the particle spectrum of SUSY has not yet been observed, suggesting that, if these particles exist, they should have an higher mass than their SM superpartners. To achieve SUSY-breaking in a way which does not reintroduce the quadratic divergences to the Higgs mass squared, a so called "soft-SUSY-breaking" term is introduced to the SUSY Lagrangian [42, 43]. This term explicitly break SUSY introducing the mass terms for Higgs, gauginos and sfermions, as well as trilinear coupling terms between sfermions and Higgs bosons. In general, if intergenerational mixing and complex phases are allowed, the soft-SUSY-breaking terms will introduce a huge number of unknown parameters $\mathcal{O}(100)$ [44]. However, in absence of phases and mixing, and if the soft terms obey a set of boundary conditions [42, 43], only few new parameters are introduced $\mathcal{O}(10)$.

1.2.2 The Higgs Sector in the MSSM

In the MSSM two doublets of complex scalar field of opposite hypercharge are required to break the electroweak symmetry, this requirement is necessary to generate masses separately for isospin up-type fermion and down-type fermions [34, 45, 46] and to cancel chiral anomalies that otherwise would spoil the renormalizability of the theory [47]. The two Higgs doublet are:

$$H_1 = \begin{pmatrix} H_1^0 \\ H_1^- \end{pmatrix} \text{ with } Y_{H_1} = -1, \qquad H_2 = \begin{pmatrix} H_2^+ \\ H_2^0 \end{pmatrix} \text{ with } Y_{H_2} = +1 \tag{1.3}$$

In analogy with the SM, a similar Higgs mechanism is employed in the MSSM [36,48] requiring that the minimum of the Higgs potential breaks $SU(2)_L \otimes U(1)_Y$ group while preserving the electromagnetic symmetry $U(1)_Q$. The neutral components of the two Higgs field acquire vacuum expectation values:

$$\langle H_1^0 \rangle = \frac{v_1}{\sqrt{2}}, \qquad \langle H_2^0 \rangle = \frac{v_2}{\sqrt{2}} \tag{1.4}$$

Three of the original eight degrees of freedom of the scalar fields are absorbed by the $W^\pm$ and Z bosons, which acquire their longitudinal polarisations and masses. The remaining degrees of freedom correspond to five scalar Higgs bosons: two CP-even and neutral h and H, a neutral CP-odd boson A and a pair of charged bosons $H^\pm$. Six parameters describes the MSSM Higgs sector: M_h, M_H, M_A, $M_{H^\pm}$, β and α, where the latter represents the mixing angle in the neutral CP-even sector, while $\tan\beta$ is equal to the ratio between the two vacuum expectation values $\tan\beta = v_1/v_2$. At tree level, only two of these parameters are actually independent, a common choice is to keep $\tan\beta$ and M_A as free the parameters of the Higgs sector. At tree level, the supersymmetric structure of the theory impose a strong hierarchical

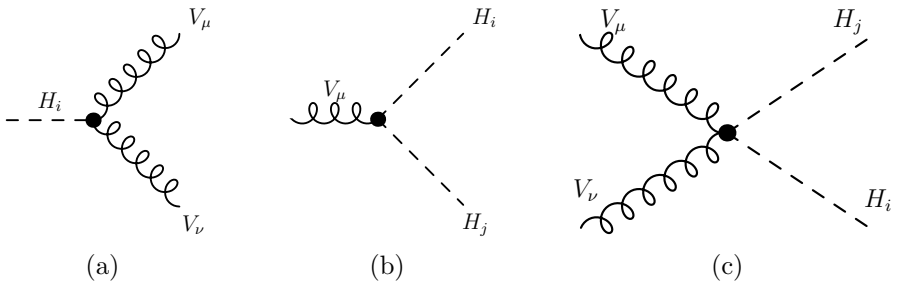

Figure 1.1: Feynman diagrams for the couplings between one Higgs boson and two gauge bosons (a), two Higgs bosons and one gauge boson (b) and two Higgs bosons and two gauge bosons (c). Based on [3].

structure on the Higgs bosons mass spectrum: the h boson is the lightest with $M_h < M_Z$, while $M_A < M_H$ and $M^2_{H^\pm} = M^2_A M^2_W$. Furthermore, the following relation holds between the mixing angles:

$$\cos^2(\beta - \alpha) = \frac{M_h^2(M_Z^2 - M_h^2)}{M_A^2(M_H^2 - M_h^2)} \tag{1.5}$$

These relations are broken by large radiative corrections to the Higgs bosons masses [49], which cause the constraint on the mass of h to move from the tree level value of M_Z to $M_h \lesssim 140$ GeV. Another restriction, coming from GUT assumptions gives $1 \lesssim \tan\beta \lesssim m_t/m_b$ [50].

1.3 Neutral Higgs Bosons Phenomenology in the MSSM

1.3.1 MSSM Higgs Couplings with SM Particles

The phenomenology of the MSSM Higgs bosons depends on their couplings with standard model and supersymmetric particles, a short overview of the former, based on the Reference [3], is given in this section.

The possible couplings between MSSM Higgs bosons and vector bosons are: the three-linear couplings $V_\mu V_\nu H_i$ among one Higgs boson and two gauge bosons and $V_\mu H_i H_j$ among one gauge boson and two Higgs bosons, as well as the couplings between two Higgs bosons and two gauge bosons $V_\mu V_\nu H_i H_j$. Figure 1.3.1 shows the Feynman diagram relative to these couplings. Among all of them, the most relevant for MSSM Higgs phenomenology are the trilinear couplings between two gauge bosons and one Higgs boson $V_\mu V_\nu H_i$. For this case, since the photon is massless, there are no Higgs-$\gamma\gamma$ and Higgs-$Z\gamma$ couplings at tree level. CP-invariance also forbids WWA, ZZA and $WZH^\pm$ couplings. Then, for the $V_\mu V_\nu H_i$ couplings, only the following possibilities remains:

$$Z_\mu Z_\nu h \;:\; ig_z M_Z \sin(\beta-\alpha) g_{\mu\nu}, \qquad Z_\mu Z_\nu H \;:\; ig_z M_Z \cos(\beta-\alpha) g_{\mu\nu} \tag{1.6}$$

$$W^+_\mu W^-_\nu h \;:\; ig_w M_W \sin(\beta-\alpha) g_{\mu\nu}, \quad W^+_\mu W^-_\nu H \;:\; ig_w M_W \cos(\beta-\alpha) g_{\mu\nu} \tag{1.7}$$

The couplings of the neutral CP-even Higgs bosons h and H with pair of vector bosons are proportional to $\sin(\beta-\alpha)$ and $\cos(\beta-\alpha)$ respectively, where $\cos(\beta-\alpha)$ is fixed at tree level following equation (1.5). An interesting phenomenological consequence is that, calling G_{VVh} and G_{VVH} the coupling between two generic vector bosons and one of the neutral CP-even Higgs bosons the following equation holds:

$$G^2_{VVh} + G^2_{VVH} = g^2_{VVH_{SM}} \tag{1.8}$$

The equations (1.7) and (1.8) leads to the fact that the couplings with vector bosons for h (H) increase (decrease) with $\tan\beta$. For relatively large value of $\tan\beta$, h has SM-like couplings with vector bosons while H decouple from them. For an overview of all the other couplings between vector bosons and Higgs bosons, charged Higgs, trilinear and quartic coupling between Higgs bosons and couplings to SUSY particles refer to Reference [3].

The MSSM Higgs bosons couplings with isospin up-type u, and down-type d fermions also depend on $\tan\beta$ and may be written as follows:

$$\begin{aligned}
G_{huu} &\propto m_u[\sin(\beta-\alpha)+\cot\beta\cos(\beta-\alpha)], & G_{hdd} &\propto m_u[\sin(\beta-\alpha)-\tan\beta\cos(\beta-\alpha)]\\
G_{Huu} &\propto m_u[\cos(\beta-\alpha)-\cot\beta\sin(\beta-\alpha)], & G_{Hdd} &\propto m_d[\cos(\beta-\alpha)+\tan\beta\sin(\beta-\alpha)]\\
G_{Auu} &\propto m_u\cot\beta, & G_{Add} &\propto m_d\tan\beta
\end{aligned}$$

The couplings with down-type (up-type) fermions of either the h or H boson is enhanced (suppressed) by a factor $\tan\beta$, depending on the magnitude of $\cos(\beta-\alpha)$ or $\sin(\beta-\alpha)$, while the coupling of A boson with down-type (up-type) fermions are directly enhanced (suppressed) by $\tan\beta$.

1.3.2 MSSM Higgs Benchmark Scenarios

At tree level, the MSSM Higgs bosons masses, decay branching fraction and production cross section are all determined by two parameters, by convention chosen to be M_A and $\tan\beta$. As it has been pointed out in Section 1.2.2, radiative corrections contribute significantly to the MSSM Higgs bosons masses and the prediction of physics observables becomes dependent on several MSSM parameters [49]. The main corrections arises from the top-stop (s)quark sector and for large $\tan\beta$ also the bottom-sbottom (s)quark sector becomes increasingly important. Furthermore, these corrections are dependent on the SUSY-breaking scale M_{SUSY}, the trilinear Higgs-stop, Higgs-sbottom Yukawa couplings, the electroweak gaugino and gluino mass parameters.

Due to the large number of free parameters, a complete scan of the MSSM parameter space is impractical in experimental analysis and phenomenological studies. To cope with this difficulty several benchmark scenarios has been proposed [4, 52], where the SUSY parameters entering via radiative corrections are fixed to particular benchmark values which exhibit interesting features of the MSSM Higgs phenomenology, while the parameters M_A and $\tan\beta$ are left free to vary. Usually results are presented in a $M_A - \tan\beta$ plane.

The m_h^{max} benchmark scenario [51] was used in the past searches for neutral MSSM Higgs bosons performed at LEP, Tevatron and LHC [64–67]. In this benchmark scenario the parameters that contributes to radiative corrections are fixed

such that the mass of the light CP-even Higgs boson, M_h, is maximal under the variation of M_A and $\tan\beta$. The m_h^{max} scenario allows to set conservative lower bounds on M_A, $M_H^{\pm}$ and $\tan\beta$ [52]. However, given the recent discovery of a Higgs boson with mass ~ 126 GeV, this scenario tend to predict a too high mass for M_h, resulting to be, for large regions of the MSSM parameter space, inconsistent with this observation. This scenario is still currently used in the presented analysis since it offer the possibility to compare results with past experiments.

Recently, several benchmark scenarios has been updated [4] to accommodate the experimental constraints on past neutral MSSM Higgs searches and the observation of a SM-like Higgs boson. An interesting updated benchmark scenario is the m_h^{mod} scenario, which has the feature to predict $M_h \simeq 125.5 \pm 3$ GeV for large region of MSSM parameter space. The m_h^{mod} scenario configuration is obtained by reducing the amount of mixing in the stop sector with respect to the m_h^{max} scenario. This can be done for both signs of the MSSM parameter that regulate the stop mixing X_t, giving rise to two complementary scenarios m_h^{mod+} and m_h^{mod-}. The difference between these two scenarios is found to be negligible for experimental searches, the m_h^{mod+} benchmark scenario has been used throughout this thesis as reference scenario.

Other interesting benchmark scenario are the light stop scenario and the light stau scenario. The first may lead to relevant modification of the gluon fusion production cross section, while the second leads to modification of the di-photon decay branching fraction of the light CP-even MSSM Higgs boson. For an overview of other relevant benchmark scenarios refer to Reference [4].

1.3.3 Neutral MSSM Higgs Bosons Production and Decay at LHC

For large region of the MSSM parameter space a SM-like Higgs boson is expected, this role is commonly played by the lightest CP-even Higgs boson, h. Given the Higgs bosons couplings discussed in Section 1.3.1 turns out that the MSSM Higgs bosons H and A tend to be degenerate in mass and decouple from gauge bosons. Furthermore the coupling of the latter two Higgs bosons with down (up) type fermions are enhanced (suppressed) by $\tan\beta$, therefore, for large $\tan\beta$ bottom-quark and τ lepton will play an important role for the Higgs bosons production and its decays.

The production of the neutral CP-even MSSM Higgs bosons at hadron colliders proceeds via the same processes as for the SM Higgs production. The pseudoscalar A, instead, cannot be produced in association with gauge bosons or in vector boson fusion (VBF) processes at tree-level, as this coupling is forbidden due to CP-invariance. At the LHC one of the most relevant production mechanisms for the MSSM Higgs bosons is gluon fusion, $gg \to A/H/h$. In addition, the production in association with b-quarks becomes important for large value of $\tan\beta$. These are the only two production mechanism that are considered in the presented analysis. Figure 1.2 shows the Feynman-diagram for these processes, while Figure 1.3 shows the production cross section of the neutral MSSM Higgs bosons via these two processes in the m_h^{max} scenario.

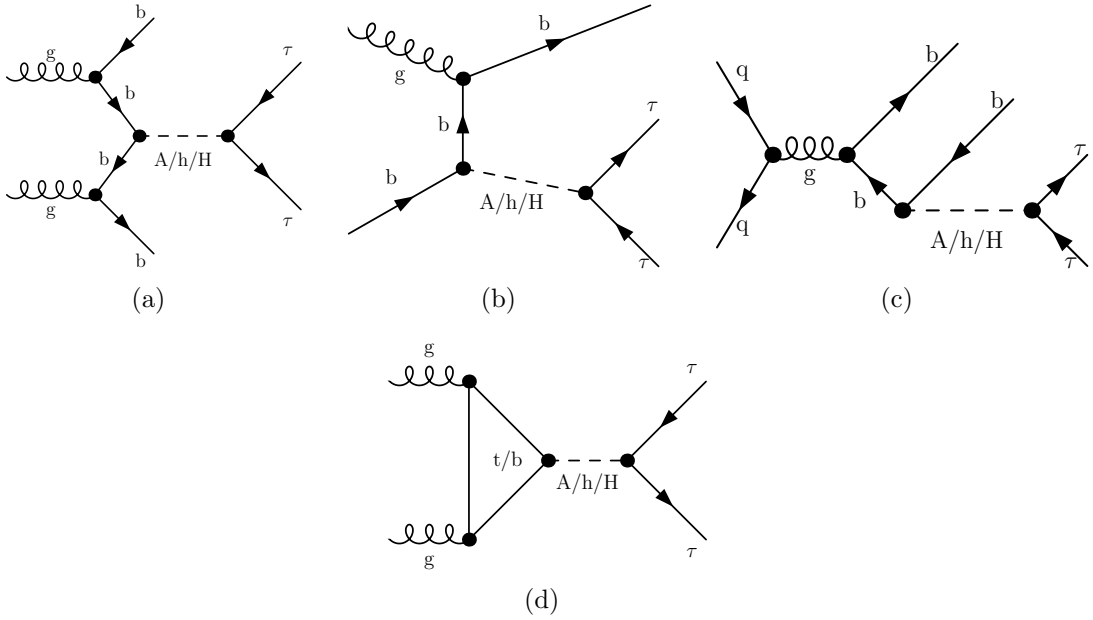

Figure 1.2: Feynman diagram for the production of the neutral MSSM Higgs bosons in association with b-quarks (a,b,c) and via gluon fusion (d) processes, subsequent decay in tau lepton pairs is considered.

The decays of the neutral MSSM Higgs bosons (in the assumption that all supersymmetric particle are heavy enough) are the same as for the SM one with the already cited exception of A. Figure 1.3 shows the decay branching fractions in the m_h^{mod+} scenario for h, H and A as a function of the mass of A for two values of $\tan\beta$. The decay into tau lepton pairs is the most important after $b\bar{b}$ and the one used in this thesis.

1.3.4 Current Status of the Search for Neutral MSSM Higgs Bosons

The measure of the couplings of the observed SM-like Higgs boson can shed light on the Higgs sector and determine if this boson is fully responsible for the generation of all the SM particles masses. There are two approaches to explore the Higgs sector: one, is to use the measured Higgs couplings with SM particles to set constraint on new physics, while the other is to directly search for additional Higgs bosons in a well defined model.

In case the SM-like Higgs boson is interpreted as the light CP-even Higgs boson of the MSSM, the couplings of the Higgs boson to vector bosons (k_V), up-type fermions (k_u) and down-type fermions (k_d), can be expressed as a function of m_A and $\tan\beta$ and this allow to set exclusion limits in the $m_A - \tan\beta$ plane [53]. Figure 1.5 shows the exclusion limits in a "simplified MSSM" model [54, 55] via fits to the measured rates of Higgs boson production and decay.

The current latest constraint on $m_A - \tan\beta$ by direct search of neutral MSSM Higgs bosons [] are shown in Figure 1.6 and are part of the work of this thesis.

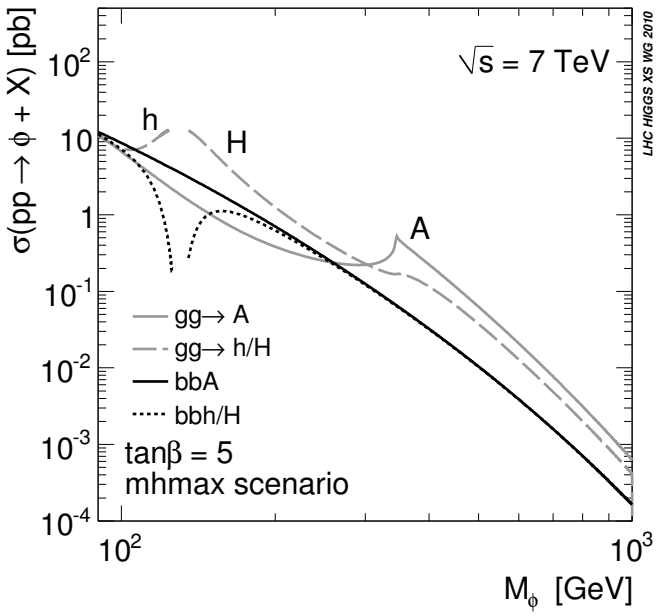

(a)

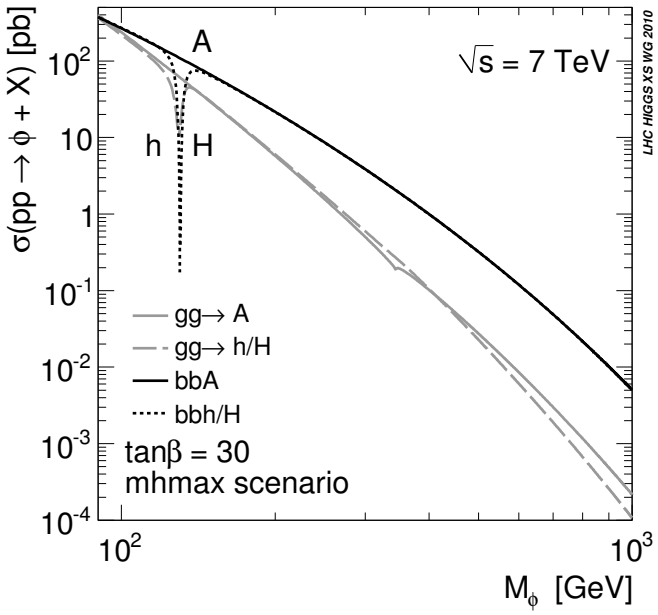

(b)

Figure 1.3: Central predictions for the total MSSM Higgs bosons production cross sections via gluon fusion and Higgs radiation off bottom quarks for $\sqrt{s} = 7$ TeV using NNLO and NLO MSTW2008 PDFs m_h^{max} scenario; (a) $\tan\beta = 5$, (b) $\tan\beta = 30$. Reference [5].

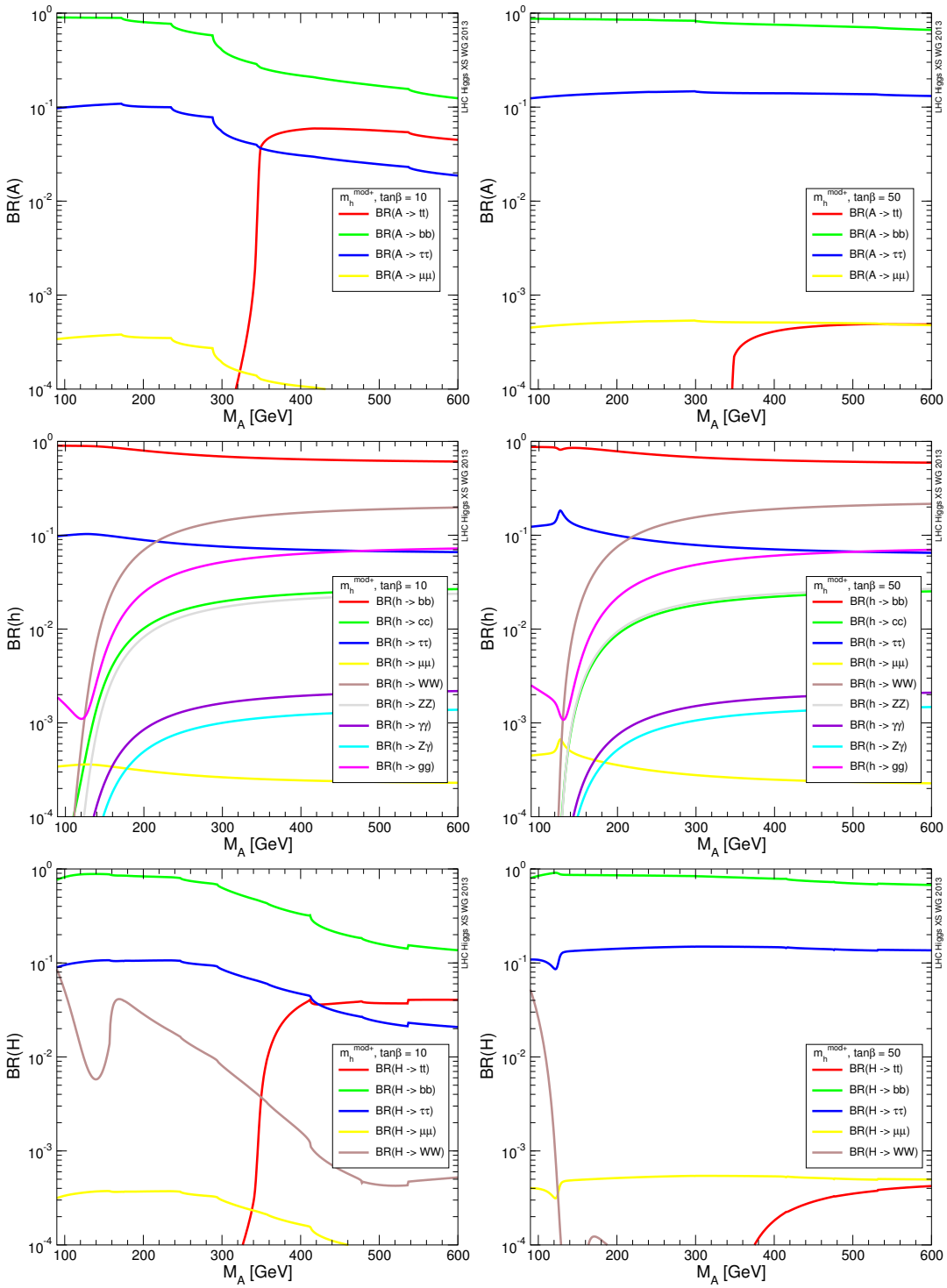

Figure 1.4: Branching fraction for the MSSM neutral Higgs bosons, $h/H/A$, in the m_h^{mod+} scenario for $\tan\beta = 10$ and $\tan\beta = 50$. Reference [4].

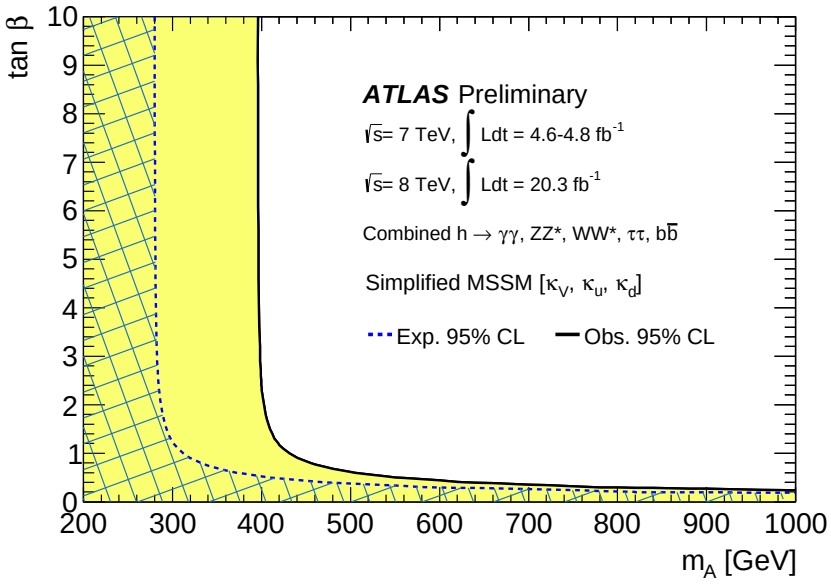

Figure 1.5: Regions of the $m_A - \tan\beta$ plane excluded in a simplified MSSM model via fits to the measured rates of Higgs boson production and decays. The likelihood contours where $2\ln\Lambda = 6.0$, corresponding approximately to 95% CL (2σ), are indicated for the data and expectation assuming the SM Higgs sector. The light shaded and hashed regions indicate the observed and expected exclusions, respectively. The SM decoupling limit is $m_A \to \infty$. See Reference [53].

Figure 1.6: Limit CMS or ATLAS depending if we manage to publish in time

Chapter 2

The ATLAS Detector at the LHC

The Large Hadron Collider (LHC) located at the European Organization for Nuclear Research (CERN) is the largest particle collider facility in the world. The ATLAS experiment is one of the several experiment situated at the LHC, it is a general-purpose detector dedicated to explore a wide range of physics topics, from precision measurements of known Standard Model processes to the search for physics beyond the Standard Model. Proton-proton collision data recorded by the ATLAS experiment has been used in this thesis for the search for the neutral MSSM Higgs bosons.

This chapter is organised as follows: the design and performance of the LHC are summarised in Section 2.1 (based on Reference [56]), while a description of the ATLAS detector is given in Section 2.2 (based on Reference [57]).

2.1 The Large Hadron Collider

The LHC is a superconducting hadron synchrotron collider. It is installed in the tunnel of the former LEP electron-positron collider and has ~ 27 km circumference. LHC is designed to collide proton beams with a centre-of-mass energy of 14 TeV and an unprecedented luminosity of $10^{34}\ cm^{-2}s^{-1}$. It can also collide heavy ions (lead) with an energy of 2.8 TeV per nucleon and a peak luminosity of $10^{27}\ cm^{-2}s^{-1}$.

The LHC provides proton-proton collision for several experiments, the most relevant for the physics program are the ATLAS, CMS [59], LHCb [60] and ALICE [61] experiments. Figure 2.1 shows the layout of the CERN accelerator complex, the protons follows several acceleration steps before injection in the LHC machine. First a linac accelerator (*Linac* 2) accelerates the protons to an energy of 50 MeV, then they are injected in the *booster* which accelerates them further to 1.4 GeV. The energy is increased to 25 GeV and successively to 450 GeV by means of two synchrotron accelerators, the *Proton Synchrotron* (PS) and the *Super Proton Synchrotron* (SPS). Finally, two proton beams are injected with opposite direction into the LHC where they reach their final energy.

The LHC beams are constituted by bunches of protons which are housed in two separate vacuum pipes. Radiofrequency cavities are employed to accelerate the protons, while superconducting magnets bends and focuses the bunches. The LHC is designed to accelerate up to 2835 bunches per beam, each of them containing $\sim 10^{11}$ protons. The nominal bunch spacing allows collision every 25 ns representing a real challenge for any read-out electronics.

In 2010, fist collisions took place at the LHC between proton beams of energy of 3.5 TeV. The LHC was successfully in operation during years 2011 and 2012, beam of protons were initially delivered with energies of 3.5 TeV which was increased to 4 TeV in 2012. Peak luminosities of about $4 \times 10^{33}\ cm^{-2}s^{-2}$ and $8 \times 10^{33}\ cm^{-2}s^{-2}$ have been reached during years 2011 and 2012 respectively. The ATLAS experiment recorded in fully operational conditions an integrated luminosity of 4.57 fb^{-1} during year 2011, while an integrated luminosity of 20.3 fb^{-1} was recorded during year 2012. Data recordered during these two years led to one of the major milestone in particle physics, the discovery in 2012 of a Higgs boson.

2.2 The ATLAS Detector

The ATLAS detector is a multi-purpose detector which aim to explore a wide range of physics topics. The physics programme of the ATLAS experiment ranges from precision measurements of known Standard Model processes to the search for physics beyond the Standard Model in a large variety of scenarios. The ATLAS detector is designed to satisfy the tight requirements on particle identification and measurements accuracy imposed by the physics goals. A schematic view of the ATLAS detector is shown in Figure 2.2. ATLAS is $44\,m$ long and $25\,m$ high, it has a typical design for a collider experiments with a forward-backward symmetry with respect the interaction point. It consist of four sub-detector which are built cylindrically around the beam pipe, going from the inside to outside they are: an Inner Detector tracker, an electromagnetic calorimeter, an hadronic calorimeter and finally a muon

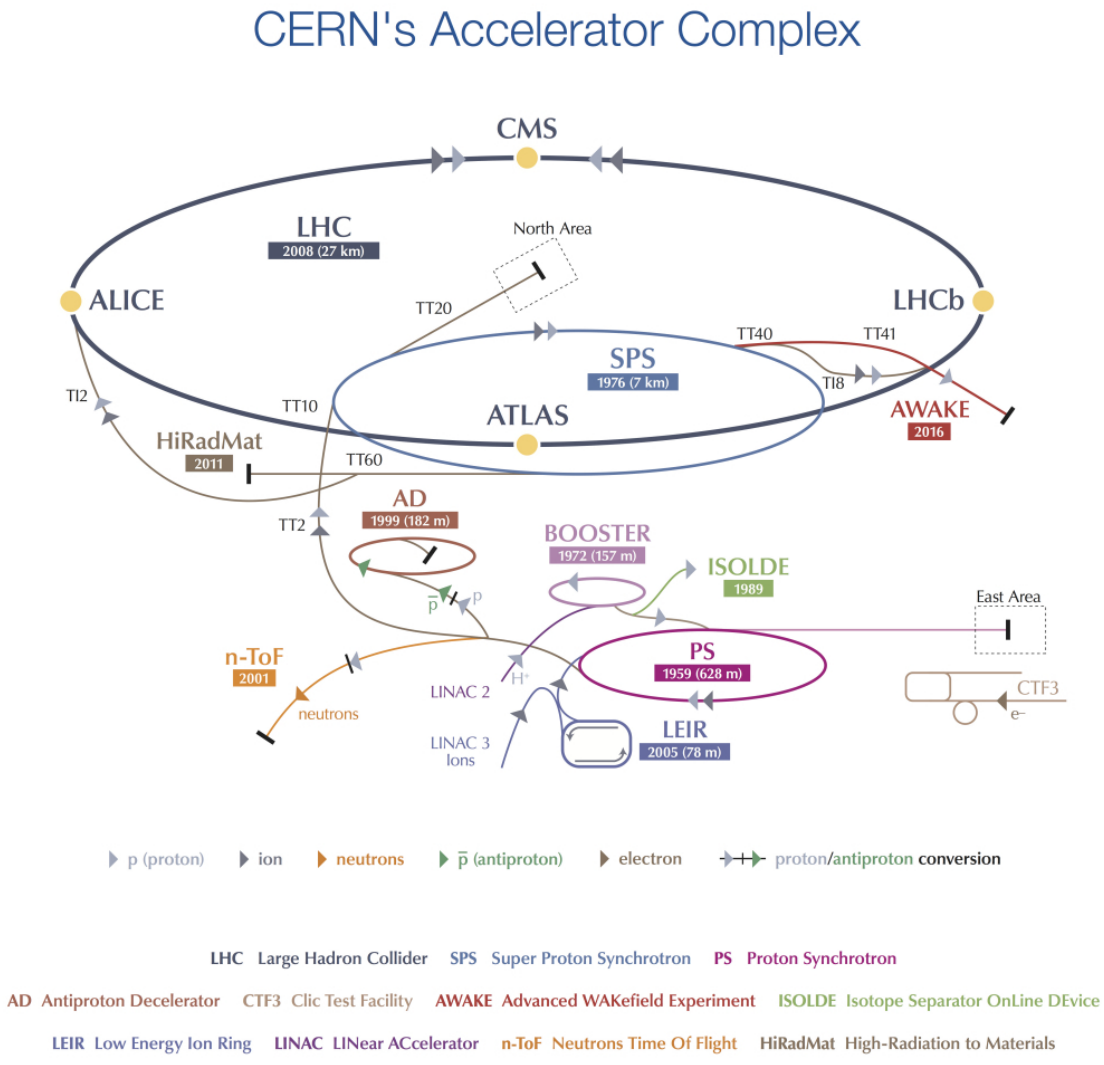

Figure 2.1: Illustration of the CERN accelerator complex [58]. The acceleration of protons starts with Linac2 followed by the acceleration in the Booster. The Proton Synchrotron (PS) and the Super Proton Synchrotron (SPS) accelerate further the protons before final injection into the LHC machine.

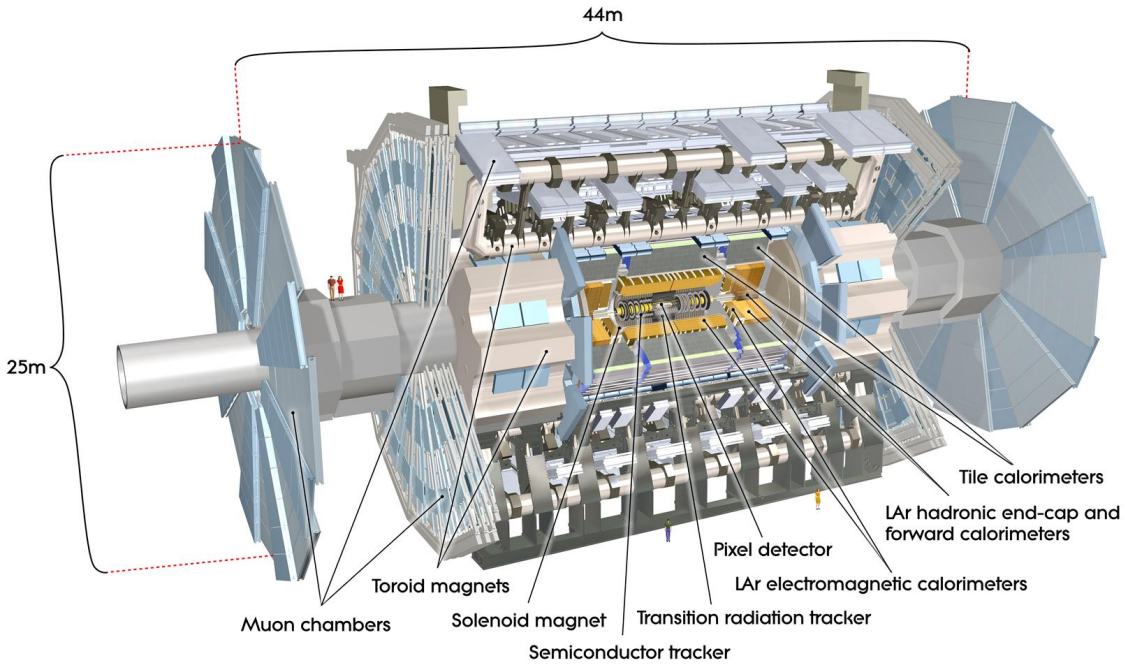

Figure 2.2: Cut-away view of the ATLAS detector with its sub-detectors system. Reference [57].

spectrometer surrounds the whole experiment. Each of these sub-detector is briefly described in what follows based on Reference [57].

2.2.1 The ATLAS coordinate system

The ATLAS coordinate system has its origin in the interaction region. The $z-$axis is pointing along the beam direction, the $y-$axis is pointing upwards and the $x-$axis towards the centre of the LHC ring. The angle ϕ is defined in the plane orthogonal to the beam axis, starting from the positive side of the $x-$axis. The angle θ is instead defined with respect to the $z-$axis. A commonly used spatial coordinate in experiments at collider is the rapidity y:

$$y \;=\; 1/2 \cdot \ln\left(\frac{E + p_z}{E - P_z}\right) \tag{2.1}$$

The difference in the rapidity of two particles is independent of Lorentz boosts along the beam axis. In the limit of β approaching to 1 or for massless particles the rapidity tend to the pseudorapidity η:

$$\eta \;=\; 1/2 \cdot \ln\left(\frac{\theta}{2}\right) \tag{2.2}$$

Given the symmetry of the ATLAS detector with respect to the interaction point, the detector is divided in two regions called *barrel* for $|\eta| \lesssim 1.5$ (depending on the

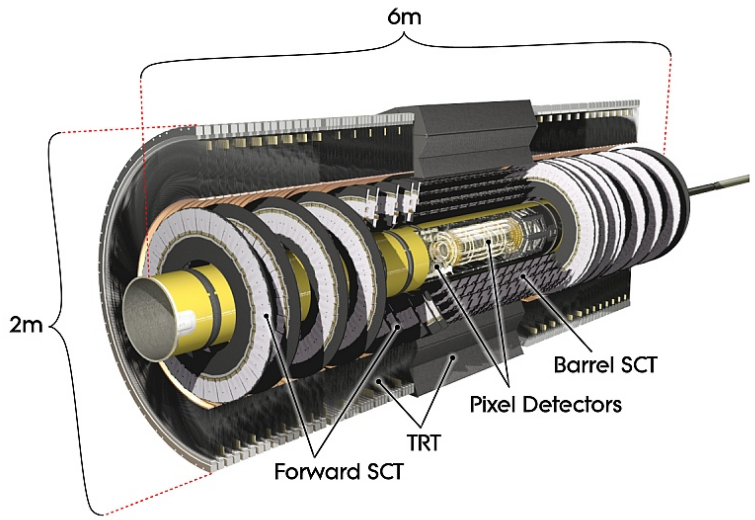

Figure 2.3: Cut-away view of the ATLAS Inner Detector tracker. Reference [57].

considered detector) and *endcap* for larger η. In ATLAS the angular separation between two particles is commonly measured by $\Delta R = \sqrt{\Delta\eta^2 + \Delta\phi^2}$.

2.2.2 The Inner Detector

The Inner Detector (ID) performs track reconstruction and momentum measurements of charged particles, it has a total length of $5.3\,m$ and a diameter of $2.5\,m$. The momentum measurement is performed by measuring the tracks curvature in a $2\,T$ magnetic field generated by a super-conducting solenoid. The layout of the Inner Detector is illustrated in Figure 2.3, it consist of three independent detector modules with fine granularity covering the region $|\eta| < 2.5$. The innermost of these detectors is the Pixel detector, which consist of three cylindrical layers of pixel silicon sensors in the barrel and three disks in the endcap region. The closest layer of pixels to the beam pipe is referred to as the B-layer. The spatial resolution of the pixel sensors is $10\,\mu m$ in the transverse and $115\,\mu m$ in the longitudinal direction with respect to the beam pipe.

The Semi-Conductor Tracker (SCT) surrounds the Pixel detector with four cylindrical layers of silicon microstrip sensor in the barrel and nine disks in the endcap region. The spatial resolution achieved by the SCT is of $17\,\mu m$ in the transverse and $590\,\mu m$ in the longitudinal direction respectively.

The outermost detector module is the Transition Radiation Tracker (TRT). It is composed of $4\,mm$ diameter Kapton straw tubes with a tungsten wire in their centre. The tube is filled with a gas mixture which allows the detection of transition radiation photons. This detector can only measure position along the transverse direction.

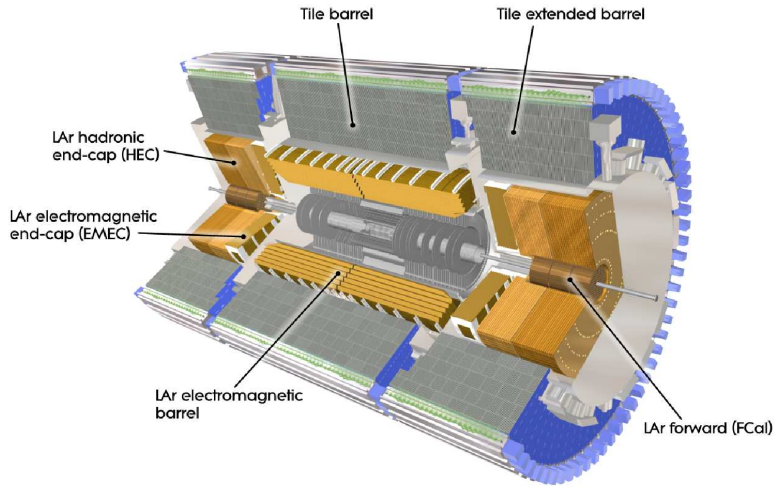

Figure 2.4: Cut-away view of the ATLAS calorimeter system. Reference [57].

2.2.3 The Calorimeter System

An illustration of the ATLAS calorimeter system is shown in Figure 2.4, it consist of an electromagnetic calorimeter (EM) surrounded by an hadronic calorimeter. These calorimeters cover the range $|\eta| < 4.9$ using different techniques suited to the widely varying radiation environment over this large $\eta-$range. Both these calorimeters are sampling calorimeters, they are builded alternating active material which performs the detector response and a passive absorber. The total detector thickness at $\eta = 0$ is 9.7 interaction length.

The EM Lar calorimeter is ideally suited for precision measurements of electrons and photons. It uses lead as absorber material and liquid argon as active material. It extends up to $|\eta| < 3.2$.

The hadronic calorimeter has a coarser granularity with respect the EM calorimeter and it is suited for jet reconstruction and missing transverse energy measurements. The hadronic calorimeter is divided in three sub-detectors which make use of different technology to cope with the changing radiation environment as a function of η. The Tile calorimeter covers region in pseudorapidity up to $|\eta| < 1.7$, it uses scintillating tiles as active material and steel as absorber. In the forward region ATLAS is instrumented with a Lar hadronic endcap calorimeter (HEC), which extends up to $|\eta| < 3.2$ and uses argon as active material and copper as absorber. The region in $3.1 < |\eta| < 4.9$ is instrumented instead with a liquid argon Forward CALorimeter (FCAL), which is divided in three modules, the closest to the interaction point uses copper as absorber material, while the other two uses tungsten.

2.2.4 The Muon Spectrometer

The muon spectrometer is instrumented with separate high-precision tracking and trigger chambers. The measure of muon momenta is performed by reconstructing the track curvature in an intense magnetic field produced by the large supercon-

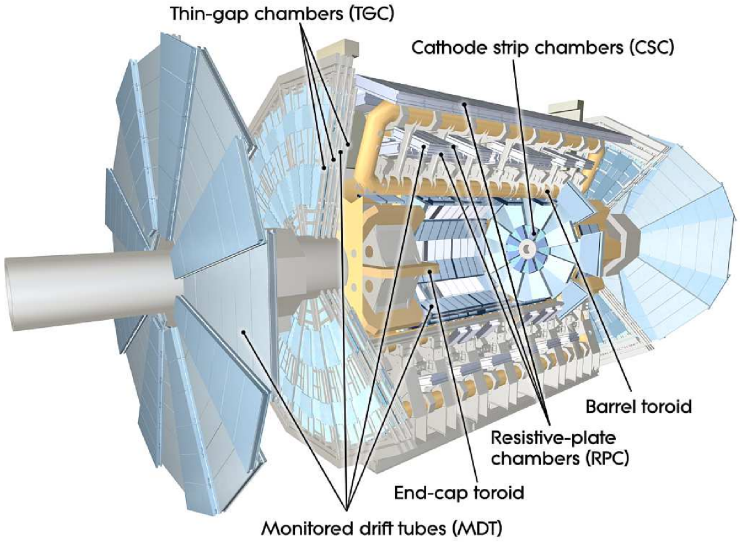

Figure 2.5: Cut-away view of the ATLAS muon spectrometer system. Reference [57].

ducting air-core toroid magnets. The layout of the muon spectrometer is shown in Figure 2.5.

Precision measurement of the track coordinates in the principal bending direction of the magnetic field is provided by Monitored Drift Tubes (MDTs) up to $|\eta| < 2.7$. Given the demanding rate and background conditions at large pseudorapidities, $2 < |\eta| < 2.7$, the innermost MDT layer is replaced by Cathode Strip Chambers (CSCs), which are multiwire proportional chambers with cathodes segmented into strips. Precise muon momentum measurement is achieved for muons with momenta up to 1 TeV. The best momentum resolution, 3-4%, is achieved for muons with transverse momenta ~ 100 GeV, while resolution of $\sim 10\%$ are reached for muons with momenta up to 1 TeV.

The trigger system covers the pseudorapidity range $|\eta| < 2.4$. Resistive Plate Chambers (RPCs) are used in the barrel and Thin Gap Chambers (TGCs) in the end-cap regions for the trigger information.

2.2.5 The Trigger System

The trigger system has three distinct levels: L1, L2, and the event filter (EF). Each trigger level refines the decisions made at the previous level and, where necessary, applies additional selection criteria.

The L1 trigger searches for high transverse-momentum muons, electrons, photons, jets, and τ leptons decaying into hadrons, as well as large missing and total transverse energy. Its selection is based on information from the set of detectors described previously. The L1 trigger defines in the interesting events one or more Regions-of-Interest (RoI), given by $\eta - \phi$ coordinates of interesting feature of the event.

The L2 selection is seeded by the RoI information provided by the L1 trigger, it uses the full granularity and precision of all the available detector data within the RoIs. The L2 triggers are designed to reduce the trigger rate to approximately 3.5 kHz.

The final stage of the event selection is carried out by the event filter, which reduces the event rate to roughly 200 Hz. Its selections are implemented using the offline analysis and reconstruction procedures described in Chapter **??**.

2.2.6 Luminosity Measurement

A precise measurement of the recordered integrated luminosity is extremely important for all the physics measurements of the ATLAS physics program.

Several technique are employed in ATLAS for the measure of the luminosity. The most relevant detectors that monitor the luminosity are the Inner Detector, the BMC and the LUCID detectors. For a detailed description of the ATLAS luminosity measurements and its performance see Reference [63]. The Inner Detector measure the luminosity by the average reconstructed proton-proton interaction per bunch crossing. The LUCID detector surrounds the beampipe on both sides of the interaction point at a distance of 17 m, providing whit its Cherenkov detectors the measures of the particle flux from the interaction point in a very forward region. The BCM counts the number of collision per bunch crossing providing an independent luminosity estimate.

Bibliography

[1] G. Altarelli, *"Collider Physics within the Standard Model: a Primer,"* arXiv:1303.2842 .

[2] S. P. Martin, *"A Supersymmetry primer,"* In *Kane, G.L. (ed.): Perspectives on supersymmetry II* 1-153 [hep-ph/9709356].

[3] A. Djouadi, *The Anatomy of Electroweak Symmetry Breaking Tome II: The Higgs Bosons in the Minimal Supersymmetric Model*, Phys. Rep. 459 (2008) 1.

[4] S. Heinemeyer *et al.* [LHC Higgs Cross Section Working Group Collaboration], "Handbook of LHC Higgs Cross Sections: 3. Higgs Properties," arXiv:1307.1347

[5] S. Dittmaier *et al.* [LHC Higgs Cross Section Working Group Collaboration], *"Handbook of LHC Higgs Cross Sections: 1. Inclusive Observables,"* arXiv:1101.0593

[6] Michael E. Peskin, Dan V. Schroeder, *An Introduction To Quantum Field Theory*, Westview Press, 1995.

[7] S. L. Glashow, Partial Symmetries of Weak Interactions, Nuc. Phys. 22 (1961) 579.

[8] A. Salam, Weak and Electromagnetic Interactions, Conf. Proc. C 680519 (1968) 367. Originally printed in Svartholm: Elementary Particle Theory, proceedings of the Nobel Symposium held 1968 at Lerum, Sweden.

[9] S. Weinberg, A Model of Leptons, Phys. Rev. Lett. 19 (1967) 1264.

[10] H. Fritsch, M. Gell-Mann, and H. Leutwyler, Advantages of the Color Octet Gluon Picture, Phys. Lett. B 47 (1973) 365.

[11] F. Englert and R. Brout, *Broken Symmetry and the Mass of Gauge Vector Mesons*, Phys. Rev. Lett. **13** (1964) 321.

[12] P. W. Higgs, *Broken symmetries, massless particles and gauge fields*, Phys. Lett. **12** (1964) 132.

[13] P. W. Higgs, *Broken Symmetries and the Masses of Gauge Bosons*, Phys. Rev. Lett. **13** (1964) 508.

[14] P. W. Higgs, *Spontaneous Symmetry Breakdown without Massless Bosons*, Phys. Rev. **145** (1966) 1156.

[15] T. W. B. Kibble, Symmetry Breaking in NonAbelian Gauge Theories, Phys. Rev. 155 (1967) 1554.

[16] The ATLAS Collaboration, *Observation of a new particle in the search for the Standard Model Higgs boson with the ATLAS detector at the LHC*, Physics Letters B **716** (2012) 1–29.

[17] The CMS Collatoration, *Observation of a new boson at a mass of 125 GeV with the CMS experiment at the LHC*, Physics Letters B **716** (2012) 30–61.

[18] W. Hollik, *"Electroweak theory,"* hep-ph/9602380.

[19] The Review of Particle Physics, J. Beringer et al. (Particle Data Group), Phys. Rev. D86, 010001 (2012) and 2013 partial update for the 2014 edition.

[20] The ALEPH, CDF, D0, DELPHI, L3, OPAL and SLD Collaborations, the LEP Electroweak Working Group, Tevatron Working Group and SLD Electroweak and Heavy Flavour Working Groups, *Precision Electroweak Measurements and Constraints on the Standard Model*, arXiv:1012.2367. Updated for 2012 winter conferences, March 2012.

[21] The Gfitter Group, M. Baak, et al., Updated Status of the Global Electroweak Fit And constraints on New Physics, Eur. Phys. J. C 72 (2012) 2003. Updated for 2012 winter conferences, March 2012, http://gfitter.desy.de.

[22] G.W. Bennett et al., Phys. Rev. Lett. 89, 101804 (2002); Erratum ibid. Phys. Rev. Lett. 89, 129903 (2002); G.W. Bennett et al., Phys. Rev. Lett. 92, 161802 (2004); G.W. Bennett et al., Phys. Rev. D73, 072003 (2006).

[23] B. Bhattacherjee, S. S. Biswal and D. Ghosh, *Top quark forward-backward asymmetry at Tevatron and its implications at the LHC*, Phys. Rev. D **83** (2011) 091501 [arXiv:1102.0545 [hep-ph]].

[24] M. Veltman, Acta. Phys. Pol. B8 (1977) 475.

[25] S. Weinberg, Gauge Hierarchies, Phys. Lett. B 82 (1979) 387.

[26] M. Veltman, The InfraredUltraviolet Connection, Acta Phys. Polon. B 12 (1981) 437.

[27] C. Smith and G. Ross, The Real Gauge Hierarchy Problem, Phys. Lett. B 105 (1981) 38.

[28] F. Zwicky, Spectral Displacement of Extra Galactic Nebulae, Helv. Phys. Acta 6 (1933) 110.

[29] E. W. Kolb and M. S. Turner, The Early Universe, Front. Phys. 69 (1990) 1.

[30] The WMAP Collaboration, D. N. Spergel et al., First Year Wilkinson Microwave Anisotropy Probe (wmap) Observations: Determination of Cosmological Parameters, Astrophys. J. Suppl. 148 (2003) 175.

[31] H. M. Georgi and S. L. Glashow, Unity of All ElementaryParticle Forces, Phys. Rev. Lett. 32 (1974) 438.

[32] J. C. Pati and A. Salam, Lepton Number as the Fourth Color, Phys. Rev. D 10 (1974) 275.

[33] P. Fayet, Phys. Lett. B 64, 159 (1976).

[34] P. Fayet, Phys. Lett. B 69, 489 (1977), Phys. Lett. B 84, 416 (1979).

[35] G.R. Farrar and P. Fayet, Phys. Lett. B 76, 575 (1978).

[36] S. Martin, in Perspectives on Supersymmetry, Ed. G.L. Kane, World Scientific, Singa- pore, 1998, hep-ph/9709356.

[37] For reviews on the MSSM, see: P. Fayet and S. Ferrara, Phys. Rep. 32 (1977) 249; H.P. Nilles, Phys. Rep. 110 (1984) 1; R. Barbieri, Riv. Nuovo Cim. 11N4 (1988) 1; R. Arnowitt and Pran Nath, Report CTP-TAMU-52-93; J. Bagger, Lectures at TASI-95, hep-ph/9604232.

[38] H. E. Haber and G. Kane, Phys. Rep. 117 (1985) 75.

[39] M. Drees and S. Martin, CLTP Report (1995) and hep-ph/9504324.

[40] D.J.H. Chung, L.L. Everett, G.L. Kane, S.F. King, J. Lykken and L.T. Wang, Phys. Rept. 407 (2005) 1.

[41] M. Drees, R.M. Godbole and P. Roy, Theory and Phenomenology of Sparticles, World Scientific, Spring 2004.

[42] L. Girardello and M.T. Grisaru, Nucl. Phys. B194 (1982) 65.

[43] Y. Okada, M. Yamaguchi and T. Yanagida, Prog. Theor. Phys. 85 (1991) 1; ibid. Phys. Lett. B262 (1991) 54; J.R. Ellis, G. Ridolfi and F. Zwirner, Phys. Lett. B257 (1991) 83; ibid. Phys. Lett. B262 (1991) 477; H.E. Haber and R. Hempfling, Phys. Rev. Lett. 66 (1991) 1815.

[44] A. Djouadi and S. RosiersLees (conv.) et al., Summary Report of the MSSM Working Group for the GDRSupersym trie, hep-ph/9901246.

[45] K. Inoue, A. Komatsu and S. Takeshita, Prog. Theor. Phys 68 (1982) 927; (E) ibid. 70 (1983) 330.

[46] E. Witten, Nucl. Phys. B188 (1981) 513; ibid Nucl. Phys. B202 (1982) 253; N. Sakai, Z. Phys. C11 (1981) 153; S. Dimopoulos and H. Georgi, Nucl. Phys. B193 (1981) 150; R.K. Kaul and P. Majumdar, Nucl. Phys. B199 (1982) 36.

[47] J.F. Donoghue and L.F. Li, Phys. Rev. 19 (1979) 945.

[48] J.F. Gunion and H.E. Haber, Nucl. Phys. B278 (1986) 449.

[49] J.F. Gunion and H.E. Haber, Nucl. Phys. B272 (1986) 1; (E) hep-ph/9301205.

[50] M. Frank et al., The Higgs Boson Masses and Mixings of the Complex MSSM in the FeynmanDiagrammatic Approach, JHEP 0702 (2007) 47.

[51] M. Carena, S. Heinemeyer, C. E. M. Wagner, and G. Weiglein, *Suggestions for benchmark scenarios for MSSM Higgs boson searches at hadron colliders*, Eur. Phys. J. **C26** (2003) 601–607, `hep-ph/0202167`.

[52] S. Heinemeyer, O. Stal, and G. Weiglein, *Interpreting the LHC Higgs Search Results in the MSSM*, Phys. Lett. B 710 (2012) 201206, arXiv:1112.3026.

[53] The ATLAS Collaboration , *Constraints on New Phenomena via Higgs Boson Coupling Measurements with the ATLAS Detector.* ATLAS-CONF-2014-010.

[54] L. Maiani, A. Polosa, and V. Riquer, Bounds to the Higgs Sector Masses in Minimal Supersymmetry from LHC Data, arXiv:1305.2172.

[55] A. Djouadi, L. Maiani, G. Moreau, A. Polosa, J. Quevillon, et al., The post-Higgs MSSM scenario: Habemus MSSM?, arXiv:1307.5205.

[56] L. Evans and P. Bryant, *LHC Machine*, JINST **3** (2008) S08001.

[57] The ATLAS Collaboration, G. Aad et al., *The ATLAS Experiment at the CERN Large Hadron Collider*, JINST **3** (2008) S08003.

[58] J. Haffner, *The CERN accelerator complex*, OPEN-PHO-ACCEL-2013-056.

[59] CMS Collaboration, CMS technical proposal, CERN-LHCC-94-38.

[60] LHCb Collaboration, LHCb technical proposal, CERN-LHCC-98-004.

[61] ALICE Collaboration, ALICE: Technical proposal for a large ion collider experiment at the CERN LHC, CERN-LHCC-95-71, CERN, 1995,

[62] G. S. Guralnik, C.R. Hagen and T. W. B. Kibble Phys.Rev.Lett. **13** (1964) 585.

[63] The ATLAS Collaboration, *Luminosity Determination in pp Collisions at $\sqrt{s} = 7$ TeV using the ATLAS Detector in 2011*, ATLAS-CONF-2011-116.

[64] ALEPH, DELPHI, L3 and OPAL Collaboration, *Search for neutral MSSM Higgs bosons at LEP*, Eur. Phys. J. **C47** (2006) 547.

[65] *Combined CDF and D0 upper limits on MSSM Higgs boson production in tau-tau final states with up to 2.2 fb^{-1} of data*, `arXiv:1003.3363 [hep-ex]`.

[66] The CMS Collaboration, S. Chatrchyan et al., `arXiv:1104.1619 [hep-ex] [hep-ex]`.

[67] The ATLAS Collaboration , *Search for the neutral Higgs bosons of the Minimal Supersymmetric Standard Model in pp collisions at $\sqrt{s} = 7$ TeV with the ATLAS detector*, `arXiv:1211.6956 [hep-ex]`.

[68] S. Heinemeyer, O. Stål and G. Weiglein, *Interpreting the LHC Higgs search results in the MSSM*, Phys.Lett. **B710** (2012) 201–206, `arXiv:1112.3026 [hep-ph]`.

[69] A. Arbey, M. Battaglia, A. Djouadi and F. Mahmoudi, *The Higgs sector of the phenomenological MSSM in the light of the Higgs boson discovery*, JHEP **1209** (2012) 107, `arXiv:1207.1348 [hep-ph]`.

[70] M. L. Mangano et al., *ALPGEN, a generator for hard multiparton processes in hadronic collisions*, JHEP **07** (2003) 001.

[71] J. Alwall et al., *Comparative study of various algorithms for the merging of parton showers and matrix elements in hadronic collisions*, Eur. Phys. J. **C53** (2008) 473, `arXiv:0706.2569`.

[72] S. Frixione and B. R. Webber, *Matching NLO QCD computations and parton shower simulations*, JHEP **06** (2002) 029, `hep-ph/0204244`.

[73] B. P. Kersevan and E. Richter-Was, *The Monte Carlo Event Generator AcerMC 2.0 with Interfaces to PYTHIA 6.2 and HERWIG 6.5*, `arXiv:0405247v1 [hep-ph]`.

[74] G. Corcella et al., *HERWIG 6: an event generator for hadron emission reactions with interfering gluons (including supersymmetric processes)*, JHEP **01** (2001) 010.

[75] J. M. Butterworth, J. R. Forshaw, and M. H. Seymour, *Multiparton Interactions in Photoproduction at HERA*, Z. Phys. **C72** (1996) 637.

[76] T. Binoth, M. Ciccolini, N. Kauer, and M. Kramer, *Gluon-induced W-boson pair production at the LHC*, JHEP **12** (2006) 046.

[77] A. S. et al., *Higgs boson production in gluon fusion*, JHEP **02** (2009) 029.

[78] T. Gleisberg et al., *Event generation with SHERPA 1.1*, JHEP **02** (2009) 007.

[79] J. Pumplin, D. R. Stump, J. Huston, H. L. Lai, P. M. Nadolsky and W. K. Tung, "New generation of parton distributions with uncertainties from global QCD analysis," JHEP **0207** (2002) 012 [hep-ph/0201195].

[80] H. -L. Lai, M. Guzzi, J. Huston, Z. Li, P. M. Nadolsky, J. Pumplin and C. -P. Yuan, "New parton distributions for collider physics," Phys. Rev. D **82** (2010) 074024 [arXiv:1007.2241 [hep-ph]].

[81] The ATLAS Collaboration, *ATLAS Monte Carlo Tunes for MC09*, ATL-PHYS-PUB-2010-002.

[82] S. Jadach, J. H. Kuhn and Z. Was, *TAUOLA - a library of Monte Carlo programs to simulate decays of polarized τ leptons*, Comput. Phys. Commun. **64** (1990) 275.

[83] E. Barberio, B. V. Eijk and Z. Was, *Photos - a universal Monte Carlo for QED radiative corrections in decays*, Comput. Phys. Commun. **66** (1991) 115.

[84] The GEANT4 Collaboration, S. Agostinelli et al., *GEANT4 - a simulation toolkit*, Nucl. Instrum. Meth. **A506** (2003) 250.

[85] The ATLAS Collaboration, G. Aad et al., *The ATLAS Simulation Infrastructure*, ATLAS-SOFT-2010-01-004, submitted to Eur. Phys. J. C., `arXiv:1005.4568`.

[86] The ATLAS Collaboration, *Estimation of $Z/\gamma^* \to \tau\tau$ Background in VBF $H \to \tau\tau$ Searches from $Z \to \mu\mu$ Data using an Embedding Technique*, ATL-PHYS-INT-2009-109.

[87] The ATLAS Collaboration, *Search for the Standard Model Higgs boson in the $H \to \tau\tau$ decay mode with 4.7 f b1 of ATLAS detactor*, Tech. Rep. ATLAS-CONF-2012-014, CERN, Geneva, Mar, 2012.

[88] The ATLAS Collaboration, *Search for the Standard Model Higgs boson $H \to \tau\tau$ decays with the ATLAS detector*, ATL-COM-PHYS-2013-722.

[89] T. S. et al., Z *physics at LEP 1*, CERN 89-08 **3** (1989) 143.

[90] The ATLAS Collaboration, Inner Detector: Technical Design Report, CERN/LHCC/97-016/017 (1997).

[91] The ATLAS Collaboration, G. Aad et al., The ATLAS Experiment at the CERN Large Hardon Collider, 2008 JINST 3 S08003.

[92] A. Bazan, T. Bouedo, P. Ghez, M. Marino and C. Tull, "The Athena data dictionary and description language," eConf C **0303241** (2003) MOJT010 [cs/0305049 [cs-se]].

[93] The ATLAS Collaboration, *Expected Performance of the ATLAS Experiment - Detector, Trigger and Physics*, CERN-OPEN-2008-020, `arXiv:0901.0512`.

[94] T. Cornelissen et al., Concepts, Design and Implementation of the ATLAS New Tracking, ATLAS Note ATL-SOFT-PUB-2007-007 (2007).

[95] Kalman, R. E. (1960). *"A New Approach to Linear Filtering and Prediction Problems".* Journal of Basic Engineering 82 (1): 3545. doi:10.1115/1.3662552

[96] The ATLAS Collaboration, Performance of primary vertex reconstruction in proton-proton collisions at $s = sqrt(7)$ TeV in the ATLAS experiment. ATLAS-CONF-2010-069.

[97] R. Fruhwirth, W. Waltenberger, P. Vanlaer, *Adaptive vertex fitting*, J. Phys. G34 (2007).

[98] The ATLAS Collaboration, *Characterization of Interaction-Point Beam Parameters Using the pp Event-Vertex Distribution Reconstructed in the ATLAS Detector at the LHC*, ATL-CONF-2010-027.

[99] The ATLAS collaboration, *Expected electron performance in the ATLAS experiment*, ATL-PHYS-PUB-2011-006

[100] The ATLAS Collaboration, *Electron reconstruction and identification efficiency measurements with the ATLAS detector using the 2011 LHC proton-proton collision data*, CERN-PH-EP-2014-040, arXiv:1404.2240

[101] The ATLAS Collaboration, G. Aad et al., *Electron performance measurements with the ATLAS detector using the 2010 LHC proton-proton collision data*, Eur.Phys.J. C72 (2012) 1909.

[102] S. Hassini, et al., *A muon identification and combined reconstruction procedure for the ATLAS detector at the LHC using the (MUONBOY, STACO, MuTag) reconstruction packages*, NIM A572 (2007) 7779.

[103] The ATLAS Collaboration, G. Aad et al., *Preliminary results on the muon reconstruction efficiency, momentum resolution, and momentum scale in ATLAS 2012 pp collision data*, ATLAS-CONF-2013-088, CERN, 2013,

[104] M. Cacciari, G. P. Salam, and G. Soyez, *FastJet user manual*, Eur.Phys.J. C72 (2012) 1896.

[105] W. Lampl et al., *Calorimeter Clustering Algorithms : Description and Performance*, ATL-LARG-PUB-2008-002.

[106] M. Cacciari, G. P. Salam, and G. Soyez, *The anti-kt jet clustering algorithm*, JHEP 04 (2008) 63.

[107] E. Abat, J. Abdallah, T. Addy, P. Adragna, et al., *Combined performance studies for electrons at the 2004 ATLAS combined test-beam*, JINST 5 (2010) P11006.

[108] ATLAS Collaboration, *Jet energy measurement with the ATLAS detector in proton-proton collisions at* $\sqrt{s} = 7$ *TeV*, Submitted to EPJ (2011) , arXiv:1112.6426

[109] The ATLAS Collaboration, *Pile-up corrections for jets from proton-proton collisions at ATLAS in 2011*, ATLAS-CONF-2012-064, July, 2012.

[110] M. Cacciari and G. P. Salam, *Pileup subtraction using jet areas*, Phys.Lett. B659 (2008) 119.

[111] The ATLAS Collaboration, G. Aad et al., *Jet energy resolution in proton-proton collisions at* $\sqrt{s} = 7$ *TeV recorded in 2010 with the ATLAS detector*, Eur.Phys.J. C73 (2013) 2306

[112] The ATLAS collaboration, *Jet energy scale and its systematic uncertainty in proton-proton collisions at* $\sqrt{s} = 7$ *TeV with ATLAS 2011 data*, ATLAS-CONF-2013-004

[113] The ATLAS Collaboration, *Data-Quality Requirements and Event Cleaning for Jets and Missing Transverse Energy Reconstruction with the ATLAS Detector in Proton-Proton Collisions at a Center-of-Mass Energy of* $\sqrt{s} = 7\ TeV$, ATLAS-CONF-2010-038.

[114] G. Piacquadio, C. Weiser, *A new inclusive secondary vertex algorithm for b-jet tagging in ATLAS*, JPCS 119 (2008) 032032

[115] The ATLAS Collaboration, G. Aad et al., *Commissioning of the ATLAS high-performance b-tagging algorithms in the 7 TeV collision data, ATLAS-CONF-2011-102*, CERN, 2011, ATLAS-CONF-2011-102.

[116] The ATLAS Collaboration, *Measuring the b-tag efficiency in a ttbar sample with 4.7* fb^{-1} *of data from the ATLAS detector* ATLAS-CONF-2012-097.

[117] The ATLAS Collaboration, *Calibration of b-tagging using dileptonic top pair events in a combinatorial likelihood approach with the ATLAS experiment* ATLAS-CONF-2014-004.

[118] The ATLAS Collaboration, *Reconstruction and Calibration of Missing Transverse Energy and Performance in Z and W events in ATLAS Proton-Proton Collisions at* $\sqrt{s}$*=7 TeV*, ATLAS-CONF-2011-080.

[119] ATLAS Collaboration, G. Aad et al., Performance of missing transverse momentum reconstruction in proton-proton collisions at 7 TeV with ATLAS, Eur.Phys.J. C72 (2012) 1844.

[120] TheATLAS Collaboration, *Performance of the Reconstruction and Identification of Hadronic tau Decays in ATLAS with 2011 Data*, ATLAS-CONF-2012-142.

[121] The ATLAS Collaboration, G. Aad et al., *Performance of the ATLAS trigger system in 2010*, Eur.Phys.J. C72 (2012) 1849.

[122] The ATLAS Collaboration, G. Aad et al., *Performance of the ATLAS muon trigger in 2011*, ATLAS-CONF-2012-099, CERN, 2012.

[123] The ATLAS Collaboration, G. Aad et al., *Performance of the ATLAS electron and photon trigger in p-p collisions at* $\sqrt{s} = 7\ TeV$ *in 2011*, ATLAS-CONF-2012-048, CERN, 2012.

[124] M. Dobbs and J.B. Hansen, *The HepMC C++ Monte Carlo Event Record for High Energy Physics*, Computer Physics Communications, ATL-SOFT-2000-001.

[125] The ATLAS Collaboration, *Evidence for the spin-0 nature of the Higgs boson using ATLAS data* , Phys. Lett. B 726 (2013), pp. 120-144.

[126] The ATLAS Collaboration, *Measurements of Higgs boson production and couplings in diboson final states with the ATLAS detector at the LHC*, Phys. Lett. B 726 (2013), pp. 88-119.

[127] The CMS Collaboration, *"Evidence for the direct decay of the 125 GeV Higgs boson to fermions,"* arXiv:1401.6527 [hep-ex].

[128] The CMS Collaboration, *Higgs boson width from on- vs. off-shell production and decay to Z-boson pairs* , arXiv:1405.3455.

[129] A. Elagin, P. Murat, A. Pranko, and A. Safonov, *A New Mass Reconstruction Technique for Resonances Decaying to di-tau*, `arXiv:1012.4686 [hep-ex]`. * Temporary entry *.

[130] T. A. Collaboration, *Search for neutral MSSM Higgs bosons decaying to $\tau\tau$ pairs in proton-proton collisions at with the ATLAS detector*, Physics Letters B **705** (2011) no. 3, 174 – 192.

[131] The ATLAS Collaboration, *Data-driven estimation of the background to charged Higgs boson searches using hadronically-decaying tau final states in ATLAS,* ATLAS-CONF-2011-051.

[132] The ATLAS Collaboration, *Measurement of the $Z \to \tau\tau$ cross section with the ATLAS detector*, Phys. Rev. D **84** (2011) 112006.

[133] T. A. Collaboration, *Search for the neutral Higgs bosons of the Minimal Supersymmetric Standard Model in pp collisions at $\sqrt{s} = 7$ TeV with the ATLAS detector*, JHEP , `arXiv:1211.6956`.

[134] Atlas statistics forum, *ABCD method in searches*, link

[135] The ATLAS Collaboration, *Search for Neutral MSSM Higgs Bosons H to $\tau\tau$ to $l\tau_h$ with the ATLAS Detector in 7 TeV Collisions*, ATL-COM-PHYS-2012-094.

[136] The ATLAS Collaboration, *Search for neutral Higgs Bosons in the decay mode $H \to \tau\tau \to ll{+}4\nu$ in proton proton collision at $\sqrt{7}$ TeV with the ATLAS Detector*, ATL-COM-PHYS-2011-758.

[137] The Atlas Collaboration, *Measurement of the ttbar production cross-section in pp collisions at $\sqrt{s} = 8$ TeV using e-mu events with b-tagged jets* . ATLAS-CONF-2013-097.

[138] T. Sjostrand, S. Mrenna and P. Skands, *PYTHIA 6.4 physics and manual*, JHEP **05** (2006) 026.

[139] A. B. et al., *Rivet user manual*, `arXiv:1003.0694 [hep-ph]`.

[140] The ATLAS and CMS Collaborations, *Procedure for the LHC Higgs boson search combination in summer 2011*, ATL-PHYS-PUB-2011-011, ATL-COM-PHYS-2011-818, CMS-NOTE-2011-005.

[141] W. Verkerke and D. P. Kirkby, *The Roofit Toolkit for Data Modeling*, eConf C0303241 (2003) MOLT007, arXiv:physics/0306116

[142] K. S. Cranmer et al., *The Roostats Project*, PoS ACAT2010 (2010) 57.

[143] K. Cranmer, G. Lewis, L. Moneta, A. Shibata, and W. Verkerke, *Histfactory: A Tool for Creating Statistical Models for use with Roofit and Roostats*, CERNOPEN2012016 (2012)

[144] E. G. G. Cowan, K. Cranmer and O. Vitells, *Asymptotic formulae for likelihood-based tests of new physics*, arXiv:1007.1727 [hep-ex].

[145] A. L. Read. *Presentation of search results: the CLs technique.* J. Phys. G: Nucl. Part. Phys., 28, 2002.

[146] A. L. Read. *Modified frequentist analysis of search results (the CLs method).* In Proceedings of the First Workshop on Confidence Limits, CERN, Geneva, Switzerland, 2000.

[147] LHC Higgs Cross Section Working Group, S. Dittmaier, C. Mariotti, G. Passarino, R. Tanaka (Eds.), et al., *Handbook of LHC Higgs Cross Sections: 1. Inclusive Observables*, arXiv:1101.0593 [hep-ph].

[148] LHC Higgs Cross Section Working Group, S. Dittmaier, C. Mariotti, G. Passarino, and R. Tanaka (Eds.), *Handbook of LHC Higgs Cross Sections: 2. Differential Distributions*, CERN-2012-002 (CERN, Geneva, 2012) , arXiv:1201.3084 [hep-ph].

[149] ATLAS collaboration *Performance of the ATLAS Silicon Pattern Recognition Algorithm in Data and Simulation at* $\sqrt{s} = 7$ *TeV*, ATLAS-CONF-2010-072

[150] The ATLAS Collaboration, *A measurement of the material in the ATLAS inner detector using secondary hadronic interactions*, arXiv:1110.6191, JINST 7 (2012) P01013

[151] The ATLAS Collaboration, *Validation of the ATLAS jet energy scale uncertainties using tracks in proton-proton collision* $\sqrt{s} = 7$ *TeV*, ATLAS-CONF-2011-067

[152] The ATLAS Collaboration, *Track Reconstruction Efficiency in* $\sqrt{s} = 7$ *TeV Data for Tracks with* $P_T > 100$ *MeV* , ATL-PHYS-INT-2010-112

[153] D. de Florian, G. Ferrera, M. Grazzini and D. Tommasini, *Transverse-momentum resummation: Higgs boson production at the Tevatron and the LHC*, JHEP **1111** (2011) , arXiv:1109.2109 [hep-ph].

[154] Statistical twiki, NuissanceCheck. https://twiki.cern.ch/twiki/bin/view/AtlasProtected/Nuisa